Original Article

Institution of MECHANICAL ENGINEERS

Journal of AEROSPACE ENGINEERING

Proc IMechE Part G:
J Aerospace Engineering
2022, Vol. 236(10) 1999–2009

DOI: 10.1177/09544100211048275
journals.sagepub.com/home/pig
SAGE

Attitude control of the low earth orbit CubeSat using a moving mass actuator

Zhengliang Lu, Yuandong Hu, Wenhe Liao and Xiang Zhang

Abstract

This paper investigates an attitude control method for the CubeSat using a moving mass actuator to solve the problem of the strong aerodynamic disturbance in low Earth orbit. The rotational and translational equations are derived for the CubeSat with three moving masses, and their dynamic effects are analyzed. A magnetorquer is used to prevent the underactuation of the attitude control system. The movement of moving masses is slowed down by using a discrete double-loop Proportion Integral Differential control method, thereby reducing the fast time-varying additional disturbance. A nonlinear observer is used for the precise estimation of the slow time-varying disturbance. Notably, the ideal attitude control torque is allocated to two actuators by using the proposed control allocation algorithm. Numerical simulation indicates that the attitude convergence accuracy is up to ±0.1° despite the uncertain dynamics, unknown disturbances, and dynamic effects. The results verify the feasibility of the proposed control method.

Keywords

Attitude control, moving masses, aerodynamic torque, disturbance observer, discrete control

Date received: 3 March 2021; revised: 30 June 2021; accepted: 26 August 2021

Introduction

Numerous CubeSat has been launched since this technology was first developed in 1999. At present, more than 55% of the CubeSat have an orbital height of less than 500 km.[1] The low Earth orbit (LEO) CubeSat has many advantages over those in a high Earth orbit,[2] such as higher imaging quality and better ground communication. However, the lower the orbit height, the stronger the impacts of environmental torques on the satellite attitude, especially the aerodynamic torque generated by the residual atmosphere in space.[3] Therefore, this study focuses on a moving mass attitude control method and proposes an integrated attitude control scheme for the LEO CubeSat using the aerodynamic torque and the magnetic torque.

The use of a set of moving masses as an attitude control actuator has been investigated.[4–8] In particular, Edwards and Kaplan[5] derived the dynamic equations for a spacecraft with one internal moving mass based on the generalized angular momentum equation. Guo and Zhao[6] analyzed the feasibility of using two moving masses to stabilize the spinning satellite and avoid errors resulting from external torques. Kumar and Zou[7] proposed an attitude control method directing using the interaction force from internal masses. The nonlinear equations of the motion were derived using the Lagrangian approach. However, in these studies, the spacecraft was simplified to be free from external forces, and only the interaction forces between the body and moving masses were investigated. This approach does not apply to the LEO satellite with strong aerodynamic forces.

The moving mass actuator also can change the external torque vector to control the attitude by modifying the vector from the center of pressure (CoP) to the center of mass (CoM).[9,10] Thomas et al.[11] and Shahin et al.[12] analyzed the controllability of the solar pressure torque by a moving mass mechanism on the solar sail. Wie and Murphy[13,14] presented an attitude control system based on two moving masses to control pitch and yaw motions of a solar-sail spacecraft. However, in LEO, the solar pressure is negligible compared with other external forces, especially the aerodynamic force.

For the LEO satellite, Lu[15] designed a double symmetric moving mass system for the triaxial stabilization of a 2U CubeSat. The system is underactuated as the aerodynamic torque is perpendicular to the relative flow vector. To prevent the underactuation, Chesi[16,17] first proposed to incorporate an additional actuator into the

School of Mechanical Engineering, Nanjing University of Science and Technology, Nanjing, China

Corresponding author:
Zhengliang Lu, School of Mechanical Engineering, Nanjing University of Science and Technology, Xiaolingwei Str. 200, Xuanwu District, Nanjing 210094, China.
Email: 112010115@njust.edu.cn

moving mass system to generate the torque in the direction of the orbital velocity. The control design was conducted in two steps. But this study only demonstrated the conceptual feasibility of using moving masses to control aerodynamic torques, and it did not consider the problems in practical applications.

Subsequently, Virgili-Llop et al.[18–20] analyzed the error sources of the aerodynamic model and developed a quaternion feedback control law, which considers the uncertainties of aerodynamic forces. To avoid exceeding the stroke of the moving mass actuator, the gain of the control law is significantly reduced,[21,22] or a saturation function on the actuator input is used.[23,24] These methods may result in long convergence times of the algorithm or lack of convergence. Lu et al.[25] found that the additional torque is related to the velocity and acceleration of moving masses, and it could be ignored in view of the thrust misalignment torque. However, when the moving mass actuator was considered for the LEO CubeSat, previous studies ignored the dynamic effects of masses. This type of disturbance has almost the same magnitude as the control torque[26]; thus, more works should be done on the verification of the feasibility of the moving mass actuator applied in the LEO CubeSat.

This study further verifies the feasibility of using the moving mass actuator to control the attitude of the LEO CubeSat. A combined attitude control method using the aerodynamic torque and the magnetic torque is developed, and the dynamic effects of the mass movement are considered. The attitude dynamic equations of the CubeSat with moving masses and the translational dynamic equations of masses are derived, and the mechanism of additional disturbances is analyzed. In addition, a double-loop Proportion Integral Differential (PID) control method is designed to verify the feasibility of the integrated control method. A discrete algorithm is used to slow down the movement and reduce the dynamic effects.

Modeling

The attitude control method based on moving masses can convert the aerodynamic disturbance to the attitude control torque. This method involves adjusting the CoM of the system using a moving mass actuator inside the satellite to change the vector from the CoM of the system to the CoP of the CubeSat. However, since the aerodynamic torque is located in the plane perpendicular to the velocity vector of the incoming air, the exclusive use of moving masses would result in an underactuated system.[8] The moving mass actuator has to contain three moving masses in three different axes to adjust the CoM of the system in this plane in any attitude. In this study, it is assumed that the three masses can be translated along three straight lines that are perpendicular to each other and parallel to the axes of the body coordinate system, and the CoM of the body and the centroid of the CubeSat are coincident.

Symbolic explanation

(1) The systems $O_IX_IY_IZ_I$ and $O_BX_BY_BZ_B$ denote the inertia coordinate system and the body coordinate system, respectively. O_S, O_B, and O_C are the CoM of the system (including masses), the CoM of the body (except masses), and the centroid of the CubeSat, respectively.
(2) The vector $\boldsymbol{R}$ locates O_C in the $O_IX_IY_IZ_I$ system. The vectors $\boldsymbol{r}'$ and $\boldsymbol{r}$ locate any point mass in the $O_IX_IY_IZ_I$ system and the $O_BX_BY_BZ_B$ system, respectively.
(3) The force $\boldsymbol{G}$ is the total gravity of the system (including masses). The force $\boldsymbol{F}_{B\to i}$ is the net force that the body applies to the mass i. The force $\boldsymbol{F}_p$ is the environmental force applied to the system, except for $\boldsymbol{G}$.
(4) The angular velocity vector of the $O_BX_BY_BZ_B$ system is defined as $\boldsymbol{\omega}_B$. The matrix $\boldsymbol{A}_{bi}$ denotes the direction cosine matrix from the $O_IX_IY_IZ_I$ system to the $O_BX_BY_BZ_B$ system.
(5) The mass of the system is m, which includes the masses of the body (except masses) m_B and the mass m_i.

Attitude dynamics of a satellite with moving masses

As shown in Figure 1, the vector $\boldsymbol{r}'$ can be defined as

$$\boldsymbol{r}' = \boldsymbol{R} + \boldsymbol{A}_{bi} \tag{1}$$

From the vector differentiation rule between coordinate systems, taking the time derivative of equation (1) for the $O_IX_IY_IZ_I$ system, the following is obtained:

$$\frac{d\boldsymbol{r}'}{dt} = \boldsymbol{V}_0 + \boldsymbol{A}(\boldsymbol{\omega}_B \times \boldsymbol{r} + \dot{\boldsymbol{r}})_{bi} \tag{2}$$

where $\boldsymbol{V}_0 = d\boldsymbol{R}/dt$ denotes the first derivative of $\boldsymbol{R}$ for the $O_IX_IY_IZ_I$ system. The operation $\dot{\boldsymbol{r}}$ is the first derivative for the $O_BX_BY_BZ_B$ system, and $\boldsymbol{\omega}_B \times\ \boldsymbol{r} +\ \dot{\boldsymbol{r}}$ denotes the first derivative of $\boldsymbol{r}$ for the $O_IX_IY_IZ_I$ system.

Then, taking the time derivative of equation (2), the following is obtained

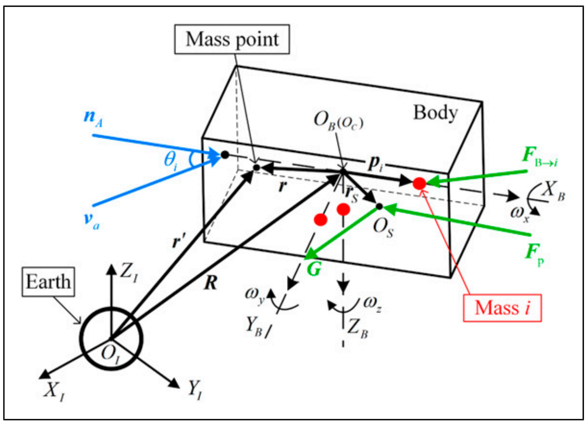

Figure 1. Force diagram of the satellite system.

$$\frac{d^2\boldsymbol{r}'}{dt^2} = \dot{\boldsymbol{V}}_0 + \boldsymbol{A}\Big[\dot{\boldsymbol{\omega}}_B \times \boldsymbol{r} + 2\boldsymbol{\omega}_B \times \dot{\boldsymbol{r}} + \ddot{\boldsymbol{r}} + \boldsymbol{\omega}_B \times (\boldsymbol{\omega}_B \times \boldsymbol{r})\Big]_{bi} \tag{3}$$

where $\dot{\boldsymbol{\omega}}_B\times\ \boldsymbol{r}+\ 2\boldsymbol{\omega}_B\times\ \dot{\boldsymbol{r}}+\ \ddot{\boldsymbol{r}}+\ \boldsymbol{\omega}_B\times\ (\boldsymbol{\omega}_B\times\ \boldsymbol{r})$ denotes the second derivative of $\boldsymbol{r}$ for the $O_IX_IY_IZ_I$ system.

Each moving mass can be considered as a point mass due to its high density and small size. The position vectors of three masses in the $O_BX_BY_BZ_B$ system are defined as $\boldsymbol{p}_1 = [l_1, \delta_{12}, \delta_{13}]^{\mathrm{T}}$, $\boldsymbol{p}_2 = [\delta_{21}, l_2, \delta_{23}]^{\mathrm{T}}$, and $\boldsymbol{p}_3 = [\delta_{31}, \delta_{31}, l_3]^{\mathrm{T}}$, respectively. Based on the theorem of momentum, the force equations of the body and mass i are defined as

$$m\frac{d^2\boldsymbol{R}}{dt^2}\sum_{i=1}^{3}\boldsymbol{F}_{B\to i}\frac{m_B}{m}p_{bibiB} \tag{4}$$

$$m_i \cdot \frac{d^2\boldsymbol{p}_i'}{dt^2} = \boldsymbol{AB}\to i\frac{m_i}{m}{}_{bi} \tag{5}$$

By combining equations (4) and (5), the force equation of the system is obtained

$$\tag{6}$$

By substituting equation (3) into equation (6), the translational dynamic equation of the system can be expressed as

$$\begin{aligned} m \cdot \dot{\boldsymbol{V}}_0 + \boldsymbol{A}\sum_{i=1}^{3}\Big[&\dot{\boldsymbol{\omega}}_B \times \boldsymbol{p}_i + 2\boldsymbol{\omega}_B \times \dot{\boldsymbol{p}}_i + \ddot{\boldsymbol{p}}_i \\ &+\boldsymbol{\omega}_B \times (\boldsymbol{\omega}_B \times \boldsymbol{p}_i)\Big]p_{bibi} \end{aligned} \tag{7}$$

Based on the generalized angular momentum equation $\boldsymbol{M} = \dot{\boldsymbol{H}}+ \boldsymbol{S}\times\ \boldsymbol{a}$,[27] the extended momentum with respect to the origin of the $O_BX_BY_BZ_B$ system expressed in the $O_BX_BY_BZ_B$ system can be written as

$$\dot{\boldsymbol{H}}_C + \boldsymbol{\omega}_B \times \boldsymbol{H}_C = \boldsymbol{M}_C + \boldsymbol{A}_{bi}^{-1} \cdot \dot{\boldsymbol{V}}_O \times \int rdm \tag{8}$$

where $\boldsymbol{M}_C$ is the moment of the environmental force relative to the CoM of the body. $\boldsymbol{H}_C$ is the angular momentum with respect to the origin of the $O_BX_BY_BZ_B$ system and can be stated as

$$\boldsymbol{H}_C = \boldsymbol{I}_B \cdot \boldsymbol{\omega}_B + \sum_{i=1}^{3} m_i\boldsymbol{p}_i \times (\boldsymbol{\omega}_B \times \boldsymbol{p}_i + \dot{\boldsymbol{p}}_i) \tag{9}$$

where $\boldsymbol{I}_B$ is inertia moment of the body.

The environmental torque in space is defined as $\boldsymbol{M}_p$. The moment of the environmental force relative to the CoM of the body is given by

$$\boldsymbol{M}_C = \boldsymbol{M}_p + \boldsymbol{r}_S \times \boldsymbol{A}_{bi}^{-1} \cdot \boldsymbol{G} \tag{10}$$

where the vector $\boldsymbol{r}_S$ locates the CoM of the system O_S in the $O_BX_BY_BZ_B$ system and is given by

$$\boldsymbol{r}_S = \frac{m_B\boldsymbol{p}_B + \sum_{i=1}^{3} m_i\boldsymbol{p}_i}{m} \tag{11}$$

where the vector $\boldsymbol{p}_B$ locates the CoM of the body in the $O_BX_BY_BZ_B$ system.

By substituting equations (9) and (10) into equation (8), the rotational dynamic equation is obtained

$$\begin{aligned} &(m \cdot \boldsymbol{r}_S) \times (\boldsymbol{A}_{bi}^{-1} \cdot \dot{\boldsymbol{V}}_O) + \boldsymbol{I}_B \cdot \dot{\boldsymbol{\omega}}_B + \boldsymbol{\omega}_B \times \boldsymbol{I}_B \cdot \boldsymbol{\omega}_B \\ &+ \sum_{i=1}^{3} m_i\Big[\boldsymbol{p}_i \times (\dot{\boldsymbol{\omega}}_B \times \boldsymbol{p}_i) + m_i\boldsymbol{p}_i \times \ddot{\boldsymbol{p}}_i + \boldsymbol{\omega}_B \times \boldsymbol{p}_i \times (\boldsymbol{\omega}_B \times \boldsymbol{p}_i) \\ &+\boldsymbol{p}_i \times (\boldsymbol{\omega}_B \times 2\dot{\boldsymbol{p}}_i)\Big] = \boldsymbol{M}_p + \boldsymbol{r}_S \times \boldsymbol{A}_{bi}^{-1} \cdot \boldsymbol{G} \end{aligned} \tag{12}$$

Subsequently, equation (7) is substituted into equation (12) to eliminate the term $\dot{\boldsymbol{V}}_0$ in equation (12), and the rotational dynamic equation of the system is converted to

$$\begin{aligned} &t\boldsymbol{I}_B\dot{\boldsymbol{\omega}}_B + \sum_{i=1}^{3} m_i\Big\{\boldsymbol{r}_S \times \boldsymbol{p}_i \times \dot{\boldsymbol{\omega}}_B + \boldsymbol{p}_i \times (\dot{\boldsymbol{\omega}}_B \times \boldsymbol{p}_i) - \boldsymbol{r}_S \\ &\times \Big[\boldsymbol{\omega}_B \times (\boldsymbol{\omega}_B \times \boldsymbol{p}_i + 2\dot{\boldsymbol{p}}_i) + \ddot{\boldsymbol{p}}_i\Big]\Big\} + \boldsymbol{\omega}_B \times \boldsymbol{I}_B\boldsymbol{\omega}_B \\ &+ \sum_{i=1}^{n} m_i\Big[\boldsymbol{p}_i \times \ddot{\boldsymbol{p}}_i + \boldsymbol{\omega}_B \times \boldsymbol{p}_i \times (\boldsymbol{\omega}_B \times \boldsymbol{p}_i) + \boldsymbol{p}_i \times (\boldsymbol{\omega}_B \times 2\dot{\boldsymbol{p}}_i)\Big] \\ &= -\boldsymbol{r}_{\mathrm{S}} \times \boldsymbol{F}_p + \boldsymbol{M}_{\mathrm{p}} \end{aligned} \tag{13}$$

By substituting equation (3) into equation (5), the motions of moving masses can be described as

$$\begin{aligned} m_i\dot{\boldsymbol{V}}_0 + \boldsymbol{A}i[&\dot{\boldsymbol{\omega}}_B \times \boldsymbol{p}_i + 2\boldsymbol{\omega}_B \times \dot{\boldsymbol{p}}_i \\ &+ \boldsymbol{\omega}_B \times (\boldsymbol{\omega}_B \times \boldsymbol{p}_i) + \ddot{\boldsymbol{p}}_i\Big]B \to i\frac{m_i}{m}{}_{bi}{}^{bi} \end{aligned} \tag{14}$$

Equation (7) is substituted into equation (14) to eliminate the term $\dot{\boldsymbol{V}}_0$ in equation (14), and the translational dynamic equation of each mass is converted to

$$\begin{aligned} &\frac{m_i}{m}\Bigg\{\Bigg(\sum_{i=1}^{3} m_i\boldsymbol{p}_y\Bigg) \times \dot{\boldsymbol{\omega}}_B - \sum_{i=1}^{3} m_i\Big[\boldsymbol{\omega}_B \times (\boldsymbol{\omega}_B \times \boldsymbol{p}_i + 2\dot{\boldsymbol{p}}_i) \\ &+\ddot{\boldsymbol{p}}_i\Big] + \boldsymbol{F}_p\{\}\Bigg\} + m_i\Big[\dot{\boldsymbol{\omega}}_B \times \boldsymbol{p}_i + 2\boldsymbol{\omega}_B \times \dot{\boldsymbol{p}}_i + \boldsymbol{\omega}_B \\ &\times (\boldsymbol{\omega}_B \times \boldsymbol{p}_i) + \ddot{\boldsymbol{p}}_i\Big] = \boldsymbol{F}_{B\to i} \end{aligned} \tag{15}$$

Since three masses are translated along three straight lines that are parallel to the axes of the body coordinate system, the forces that the body applies to each mass are expressed as

$$\begin{cases} \boldsymbol{f}_{B\to 1} = \begin{bmatrix} u_1 & f_{B\to 1y} & f_{B\to 1z} \end{bmatrix}^{\mathrm{T}} \\ \boldsymbol{f}_{B\to 2} = \begin{bmatrix} f_{B\to 2x} & u_2 & f_{B\to 2z} \end{bmatrix}^{\mathrm{T}} \\ \boldsymbol{f}_{B\to 3} = \begin{bmatrix} f_{B\to 3x} & f_{B\to 3y} & u_3 \end{bmatrix}^{\mathrm{T}} \end{cases} \tag{16}$$

where u_1, u_2, and u_3 denote the driving forces in three axes. By substituting equation (16) into equation (15), the translational dynamic equation of each mass can be described as

$$\begin{aligned} &\frac{m_i}{m}\boldsymbol{b}_i\Bigg\{\Bigg(\sum_{i=1}^{3} m_i\boldsymbol{p}_y\Bigg) \times \dot{\boldsymbol{\omega}}_B - \sum_{i=1}^{3} m_i\Big[\boldsymbol{\omega}_B \times (\boldsymbol{\omega}_B \times \boldsymbol{p}_i + 2\dot{\boldsymbol{p}}_i) \\ &+\ddot{\boldsymbol{p}}_i\Big] + \boldsymbol{F}_p\{\}\Bigg\} + m_i\boldsymbol{b}_i\Big[\dot{\boldsymbol{\omega}}_B \times \boldsymbol{p}_i + 2\boldsymbol{\omega}_B \times \dot{\boldsymbol{p}}_i \\ &+\boldsymbol{\omega}_B \times (\boldsymbol{\omega}_B \times \boldsymbol{p}_i) + \ddot{\boldsymbol{p}}_i\Big] = u_i \end{aligned} \tag{17}$$

where $\boldsymbol{b}_1 = [1, 0, 0]$, $\boldsymbol{b}_2 = [0, 1, 0]$, and $\boldsymbol{b}_3 = [0, 0, 1]$ are constant matrices. The scalar expansion form of the translational dynamic equation of each mass is shown in the Appendix.

Attitude kinematics and dynamics

The orbit coordinate system $O_O X_O Y_O Z_O$ is here defined to describe the attitude. This study defines the orbit coordinate system as the reference coordinate system, and the modified Rodrigues (MRS) parameter $\boldsymbol{\sigma}_{bo}$ is used to describe the attitude mapping from the $O_O X_O Y_O Z_O$ system to the $O_B X_B Y_B Z_B$ system. Thus, the kinematic equation for the $O_O X_O Y_O Z_O$ system based on the MRS can be expressed as

$$\dot{\boldsymbol{\sigma}}_{bo} = \boldsymbol{G}(\boldsymbol{\sigma}_{bo})\boldsymbol{\omega}_{bo} \tag{18}$$

where

$$\boldsymbol{G}(\boldsymbol{\sigma}_{bo}) = \frac{1}{2}\left(\boldsymbol{I}_{3\times3} + [\boldsymbol{\sigma}_{bo}]^{\times} + \boldsymbol{\sigma}_{bo}\boldsymbol{\sigma}_{bo}^{\mathrm{T}} - \frac{1 + \boldsymbol{\sigma}_{bo}^{\mathrm{T}}\boldsymbol{\sigma}_{bo}}{2}\boldsymbol{I}_{3\times3}\right) \tag{19}$$

with $\boldsymbol{I}_{3\times3} \in \boldsymbol{R}^{3\times3}$ denoting the identity matrix, and $[]^{\times}$ representing the cross-product operator.

The corresponding direction cosine matrix $\boldsymbol{A}_{bo}$ from the $O_O X_O Y_O Z_O$ system to the $O_B X_B Y_B Z_B$ system is given by

$$\boldsymbol{A}_{bo} = \boldsymbol{I}_{3\times3} - \frac{4\left(1 - \boldsymbol{\sigma}_{bo}^{\mathrm{T}}\boldsymbol{\sigma}_{bo}\right)}{\left(1 + \boldsymbol{\sigma}_{bo}^{\mathrm{T}}\boldsymbol{\sigma}_{bo}\right)^2}[\boldsymbol{\sigma}_{bo}]^{\times} + \frac{8}{\left(1 + \boldsymbol{\sigma}_{bo}^{\mathrm{T}}\boldsymbol{\sigma}_{bo}\right)^2}[\boldsymbol{\sigma}_{bo}]^{\times 2} \tag{20}$$

Thus, the angular velocity of the body for the $O_O X_O Y_O Z_O$ system can be expressed as

$$\boldsymbol{\omega}_{bo} = \boldsymbol{\omega}_B - \boldsymbol{A}_{bo}\boldsymbol{\omega}_{oi} \tag{21}$$

where $\boldsymbol{\omega}_{oi}$ represents the angular velocity of the $O_O X_O Y_O Z_O$ system for the $O_I X_I Y_I Z_I$ system expressed in the $O_O X_O Y_O Z_O$ system. Taking the time derivative of equation (21) and using the fact that $\dot{\boldsymbol{A}}_{bo} = -\boldsymbol{\omega}_{bo} \times \boldsymbol{A}_{bo}$ and $\dot{\boldsymbol{\omega}}_{oi} = 0$, the following is obtained

$$\dot{\boldsymbol{\omega}}_{bo} = \dot{\boldsymbol{\omega}}_B + \boldsymbol{\omega}_{bo} \times \boldsymbol{A}_{bo}\boldsymbol{\omega}_{oi} \tag{22}$$

By substituting equation (22) into equation (13), the rotational dynamic equation relative to the $O_O X_O Y_O Z_O$ system can be written as

$$\begin{aligned}
&\left[\boldsymbol{I}_B + \left[\boldsymbol{r}_S[]^{\times}\left[\sum_{i=1}^{3} m_i\boldsymbol{p}_i\right]^{\times} \sum_{i=1}^{3} m_i\left([\boldsymbol{p}_i]^{\times}\right)^2\right](\dot{\boldsymbol{\omega}}_{bo} - \boldsymbol{\omega}_{bo}\right.\\
&\left.\times \boldsymbol{A}_{bo}\boldsymbol{\omega}_{oi})\right] + \boldsymbol{\omega}_B \times \boldsymbol{I}_B\boldsymbol{\omega}_B - \sum_{i=1}^{3\Sigma} m_i\boldsymbol{r}\Big[\boldsymbol{\omega}_B \times (\boldsymbol{\omega}_B \times \boldsymbol{p}_i + 2\dot{\boldsymbol{p}}_i)\\
&+\ddot{\boldsymbol{p}}_i\Big]_S + \sum_{i=1}^{n} m_i\Big[\boldsymbol{p}_i \times \ddot{\boldsymbol{p}}_i + \boldsymbol{\omega}_B \times \boldsymbol{p}_i \times (\boldsymbol{\omega}_B \times \boldsymbol{p}_i) + \boldsymbol{p}_i\\
&\times (\boldsymbol{\omega}_B \times 2\dot{\boldsymbol{p}}_i)\Big] = -\boldsymbol{r}_S \times \boldsymbol{F}p_p
\end{aligned} \tag{23}$$

Aerodynamic model

This study only considers the aerodynamic drag in the aerodynamic model, and its direction is simplified as the reverse direction of the satellite flight. The aerodynamic parameters are calculated using the ideal model or are selected according to the empirical value.

As shown in Figure 1, the vector $\boldsymbol{n}_A$ is the inner normal unit vector of the surface i, and $\boldsymbol{v}_a$ is the velocity vector of the incoming air expressed in the $O_O X_O Y_O Z_O$ system. The angle between the vectors $\boldsymbol{n}_A$ and $\boldsymbol{v}_a$ is θ_i. Thus, the aerodynamic drag of the surface i expressed in the $O_B X_B Y_B Z_B$ system can be described as[17]

$$\boldsymbol{F}^b_{\mathrm{aero}i} = \frac{1}{2}\rho_a\|\boldsymbol{v}_a\|^2 C_D A_{pi}\cos\theta_i H(\cos\theta_i)\cdot\boldsymbol{A}_{bo}\widehat{\boldsymbol{v}}_a \tag{24}$$

where ρ_a is the mean atmospheric density; C_D is the coefficient of atmospheric drag; and A_{pi} is the area of the surface i. The vector $\widehat{\boldsymbol{v}}_a$ denotes the unit vector of $\boldsymbol{v}_a$ and is simplified as $[-1, 0, 0]^{\mathrm{T}}$. The function $H(\cos\ \theta_i)$ is used to determine whether the surface i is windward or leeward; it is defined as

$$H(\cos\theta_i) = \begin{cases} 1, & \cos\theta_i > 0, \quad \text{windward,} \\ 0, & \cos\theta_i \le 0, \quad \text{leeward.} \end{cases} \tag{25}$$

Since it is assumed that the satellite has n_s convex flat surfaces, the aerodynamic force of the system expressed in the $O_B X_B Y_B Z_B$ system can be described as

$$\boldsymbol{F}_{\mathrm{aero}} = \frac{1}{2}\rho_a\|\boldsymbol{v}_a\|^2 C_D\sum_{i=1}^{n_s}\left[A_{pi}\cos\theta_i H(\cos\theta_i)\right]\cdot\boldsymbol{A}_{bo}\widehat{\boldsymbol{v}}_a \tag{26}$$

It should be noted that the aerodynamic torque denotes the moment of the aerodynamic force relative to the CoM of the system, and the radius vector extends from the CoM of the system O_S to the CoP of the CubeSat. Since it is assumed that the satellite is completely convex, the CoP of the CubeSat O_P coincides with the centroid of the system O_C.[15] Moreover, the origin of the body coordinate system O_B is defined to coincide with the CoM of the body. Thus, the aerodynamic torque can be written as

$$\begin{aligned}
\boldsymbol{T}_{\mathrm{aero}} &= \boldsymbol{r}_{O_S\to O_P} \times \boldsymbol{F}_{\mathrm{aero}} = \boldsymbol{r}_{O_S\to O_C} \times \boldsymbol{F}_{\mathrm{aero}}\\
&= (\boldsymbol{r}_{O_S\to O_B} + \boldsymbol{r}_{O_B\to O_C}) \times \boldsymbol{F}_{\mathrm{aero}}\\
&= -\boldsymbol{r}_S \times \boldsymbol{F}_{\mathrm{aero}} + \boldsymbol{r}_{O_B\to O_C} \times \boldsymbol{F}_{\mathrm{aero}}
\end{aligned} \tag{27}$$

Considering that the aerodynamic drag is much greater than other external forces (except gravity) in LEO, the environmental force $\boldsymbol{F}_p$ can be simplified as the aerodynamic drag, that is, $\boldsymbol{F}_p \approx \boldsymbol{F}_{\mathrm{aero}}$. Moreover, the vector from the CoM of the body to the centroid of the system O_C is assumed to be negligible so that $\boldsymbol{r}_{O_B\to O_C} \to 0$; thus, the item on the right of the equal sign in equation (13) can be simplified to

$$\begin{aligned}
&-\boldsymbol{r}_S \times \boldsymbol{F}_p + \boldsymbol{M}_p \approx -\boldsymbol{r}_S \times \boldsymbol{F}_{\mathrm{aero}} + \boldsymbol{r}_{O_B\to O_C} \times \boldsymbol{F}_{\mathrm{aero}}\\
&\quad = \boldsymbol{T}_{\mathrm{aero}} = -\boldsymbol{r}_S \times \boldsymbol{F}_{\mathrm{aero}}
\end{aligned} \tag{28}$$

Model analysis

Dynamic effect of the actuator

The dynamic effect of moving masses is an inevitable additional disturbance, which can be divided into the additional moment of inertia $\boldsymbol{I}_M$ and the additional torque $\boldsymbol{M}_{xt}$. By combining the rotational equation in equation (13), the dynamic effect can be expressed as

$$\begin{cases} \boldsymbol{I}_M = [\boldsymbol{r}_s]^{\times}\left[\sum_{i=1}^{3} m_i\boldsymbol{p}_i\right]^{\times} - \sum_{i=1}^{3} m_i\left([\boldsymbol{p}_i]^{\times}\right)^2 \\ \boldsymbol{M}_{xt} = \boldsymbol{M}_a + \boldsymbol{M}_c \\ \boldsymbol{M}_a = \boldsymbol{r}_s \times \sum_{i=1}^{3} m_i\ddot{\boldsymbol{p}}_i - \sum_{i=1}^{3} m_i\boldsymbol{p}_i \times \ddot{\boldsymbol{p}}_i \\ \boldsymbol{M}_c = \boldsymbol{r}_s \times \left(2\boldsymbol{\omega}_B \times \sum_{i=1}^{3} m_i\dot{\boldsymbol{p}}_i\right) - \sum_{i=1}^{3} 2m_i\boldsymbol{p}_i \times (\boldsymbol{\omega}_B \times \dot{\boldsymbol{p}}_i) \end{cases} \tag{29}$$

where $\boldsymbol{M}_a$ is the additional inertial torque related to acceleration $\ddot{\boldsymbol{p}}_i$; $\boldsymbol{M}_c$ is the additional Coriolis torque related to velocity $\dot{\boldsymbol{p}}_i$. The use of these interaction forces has been proposed in previous studies to directly control the attitude.[7,8] However, based on the law of the conservation of the angular momentum, the attitude can only be controlled in two axes.

Due to the additional moment of inertia caused by the position changes of moving masses, the inertia principle axes of the system may be shifted, which results in a more serious coupling of control torques. It is evident in equation (29) that the additional inertia torque $\boldsymbol{M}_a$ and the additional Coriolis torque $\boldsymbol{M}_c$ change with the movement of moving masses. Thus, these two types of additional torques are fast time-varying, and might cause attitude jitters. These two additional torques can be significantly reduced by slowing down the mass movement. Moreover, although the additional gyroscopic torque always exists, it is far lower than the other additional torques and the aerodynamic control torque; therefore, the additional gyroscopic torque can be ignored. Due to the existence of these two types of disturbance torques, the attitude dynamic characteristics exhibit the strong nonlinearity, affecting the dynamic quality of the control system.

Atmospheric uncertainty

Due to the influence of the season, day and night, solar activity, temperature, and other factors, the atmospheric environment in space is challenging to predict. Thus, it is difficult to establish an accurate prediction model for the real atmospheric conditions at different positions and altitudes. Moreover, the aerodynamic torque applied to the satellite is also related to the surface material, temperature, and boundary of its body. Therefore, the aerodynamic force calculated from the existing aerodynamic model has errors in the magnitude and direction.

The directional error of the aerodynamic force is primarily attributed to the time-varying atmospheric motion. At present, the latest atmospheric motion model HWM07[28] is only based on the average value of the Earth's climate, and this model does not consider the vertical motion of the atmosphere. By using this model, it illustrates that there exists an uncertainty of ±3° in the direction of the aerodynamic force at the orbit height of 200–400 km.[18] In this study, the direction of the aerodynamic force is simplified to the reverse direction of the satellite flight, and the uncertainty of the direction is considered a source of disturbance.

The magnitude error of the aerodynamic force is primarily caused by the non-measurable coefficient of the atmospheric drag C_D and the time-varying atmospheric density ρ_a. Although the coefficient C_D is not time-varying, it is challenging to measure and can only be determined by experience within a certain range. The density ρ_a changes rapidly with the altitude of the orbit and is closely related to the time of day or night, solar activity, and position. Due to the alternation of day and night, the atmospheric density ranges from −20% to +30%.[18] Thus, the error of the average atmospheric density is the main reason for the magnitude error of the aerodynamic force.

Sources of system disturbance

The following sources of disturbance are considered:

(1) The CoM of the body is fixed, but it is difficult to measure. The simplification of using the centroid of the body as the CoM of the body leads to the unknown deviation $\triangle\boldsymbol{r}_s$.
(2) The unknown moment of the environmental force relative to the CoM of the body. If the moment of the environmental force relative to the CoM of the body $\boldsymbol{M}_p$ is ignored, a small error will occur.
(3) The additional torque caused by the motion of the moving masses $\boldsymbol{M}_{xt}$.
(4) The unknown error of the aerodynamic force in terms of magnitude and direction $\triangle\boldsymbol{F}_{aero}$.
(5) The error of the torque due to the simplification of considering the environmental forces as the aerodynamic drag $\boldsymbol{d}_s$.
(6) The error of the control input due to the stroke limitation of masses and the movement process $\boldsymbol{d}_{con}$.

Considering these disturbances and equation (29), the rotational dynamic equation in equation (23) is transformed into

$$(\boldsymbol{I}_B + \boldsymbol{I}_M)\dot{\boldsymbol{\omega}}_{bo} = -\boldsymbol{\omega}_B \times (\boldsymbol{I}_B + \boldsymbol{I}_M)\boldsymbol{\omega}_B + (\boldsymbol{I}_B + \boldsymbol{I}_M)(\boldsymbol{\omega}_{bo} \times \boldsymbol{A}_{bo}\boldsymbol{\omega}_{oi}) - \boldsymbol{r}_s \times \boldsymbol{F}_{\text{aero}} + \boldsymbol{d} \tag{30}$$

where $\boldsymbol{d}$ is the sum of the system disturbance, which is written as

$$\boldsymbol{d} = \boldsymbol{d}_s + \boldsymbol{d}_{\text{con}} + \boldsymbol{M}_{xt} + [-\boldsymbol{r}_s \times \triangle\boldsymbol{F}_{\text{aero}} - \triangle\boldsymbol{r}_s \times (\boldsymbol{F}_{\text{aero}} + \triangle\boldsymbol{F}_{\text{aero}})] \tag{31}$$

Attitude controller design

In this study, a three-axis magnetorquer is used to complement the moving mass system to obtain an ideal three-dimensional torque $\boldsymbol{u}_t$ and prevent the underactuation of the system. This method greatly decreases the residual oscillation error due to underactuation typically associated with the magnetically controlled attitude of a nano-satellite in the presence of residual aerodynamic torque.[29–31] It enables higher pointing accuracy for an LEO nano-satellite.

The torque generated by the magnetorquer is define as $\boldsymbol{T}_B$; thus, the rotational dynamic equation in equation (30) can be rewritten as

$$(\boldsymbol{I}_B+\boldsymbol{I}_M)\dot{\boldsymbol{\omega}}_{bo}=-\boldsymbol{\omega}\times(\boldsymbol{I}_B+\boldsymbol{I}_M)\boldsymbol{\omega}+(\boldsymbol{I}_B+\boldsymbol{I}_M)(\boldsymbol{\omega}_{bo}\times\boldsymbol{A}_{bo}\boldsymbol{\omega}_{oi})+\boldsymbol{u}_t+\boldsymbol{d} \tag{32}$$

where $\boldsymbol{u}_t=\boldsymbol{T}_B-\boldsymbol{r}_s\times\boldsymbol{F}_{\text{aero}}$ and $\boldsymbol{T}_B=\boldsymbol{m}_B\times\boldsymbol{B}$. $\boldsymbol{m}_B$ is the magnetic moment generated by the magnetorquer, and $\boldsymbol{B}$ is the geomagnetic vector expressed in the $O_BX_BY_BZ_B$ system.

As shown in Figure 2, a double closed-loop control scheme is designed to verify the feasibility of the moving mass actuator. In the outer loop, the control law is designed for the three-dimensional ideal control torque, and the torque is then allocated to the two actuators using a control allocation algorithm. In the inner loop, the servo control closed loop of the mass positions calculates the driving force applied to moving masses according to the position feedback.

Notably, in this study, the dynamic effect of the movement of masses is considered in the design of the control system instead of directly ignoring it like the previous studies.[17,18] A discrete PID control method is used to slow down the movement and significantly reduce the fast time-varying disturbance. Besides, a nonlinear observer is introduced to estimate the system disturbance, which is feedforward compensated in the controller.

In the discrete PID algorithm, a sampling interval is used instead of continuous sampling. Numerical integration of the rectangular method is used instead of integration, and the first-order backward difference is used instead of the differential.[32] One advantage of this method is that the differential feedback is not needed. Considering that most servo systems only have position feedback in practical implementations, the discrete PID control method is highly suitable for the position control of the internal moving mass system.

Digital PID algorithm

The stroke of each mass is strictly limited, and thus the frequent overshoot of the position could damage the moving mass actuator. When the deviation of the state is large, it may cause integral accumulation, which leads to large overshoot and multiple oscillations.[33] Therefore, in this study, the discrete PID control algorithm based on the integral separation method is used in the inner position control loop to avoid the large overshoot. The PID control law only uses the integral term when the state is close to the target.

The motor sampling sequence is define as k_M, and the period of the discrete motor control is defined as T_P. The position error of masses is defined as

$$\boldsymbol{e}_l(k_M)=\boldsymbol{L}^d(k_M)-\boldsymbol{L}(k_M) \tag{33}$$

where $\boldsymbol{L}(k_M)=[l_1,l_2,l_3]^{\mathrm{T}}$ is the position state, and $\boldsymbol{L}^d(k_M)=[l_1^d,l_2^d,l_3^d]^{\mathrm{T}}$ is the position target.

The driving force are defined as $\boldsymbol{u}(k_M)=[u_1,u_2,u_3]^{\mathrm{T}}$. Thus, the PID control law in the inner position control loop is given by

$$\boldsymbol{u}(k_M)=k_p^{\text{in}}\boldsymbol{e}_l(k_M)+\boldsymbol{\beta}k_i^{\text{in}}\sum_{j=0}^{k_M}\boldsymbol{e}_l(k_M)T_P+k_d^{\text{in}}\frac{\boldsymbol{e}_l(k_M)-\boldsymbol{e}_l(k_M-1)}{T_P} \tag{34}$$

where k_p^{in}, k_i^{in}, and k_d^{in} are the control parameters. The parameter $\boldsymbol{\beta}=\operatorname{diag}(\beta_1,\beta_2,\beta_3)$ is the coefficient matrix of the integral term related to the given threshold $\boldsymbol{\varepsilon}=[\varepsilon_1,\varepsilon_2,\varepsilon_3]^{\mathrm{T}}$ and is expressed as

$$\beta_i=\begin{cases}1 & |e_{li}(k_M)|\le\varepsilon_i\\ 0 & |e_{li}(k_M)|>\varepsilon_i\end{cases},\quad(i=1,2,3) \tag{35}$$

In the outer attitude control loop, considering the complex disturbance of the system, a nonlinear observer is used to deal with the disturbance or uncertainty rejection problem.[34] The vector $\widehat{\boldsymbol{d}}$ denotes the observed value of $\boldsymbol{d}$ and its time derivative is defined as

$$\dot{\widehat{\boldsymbol{d}}}=K\big(\boldsymbol{d}-\widehat{\boldsymbol{d}}\big) \tag{36}$$

where $K>0$ is the gain of the observer and is related to the observer convergence.

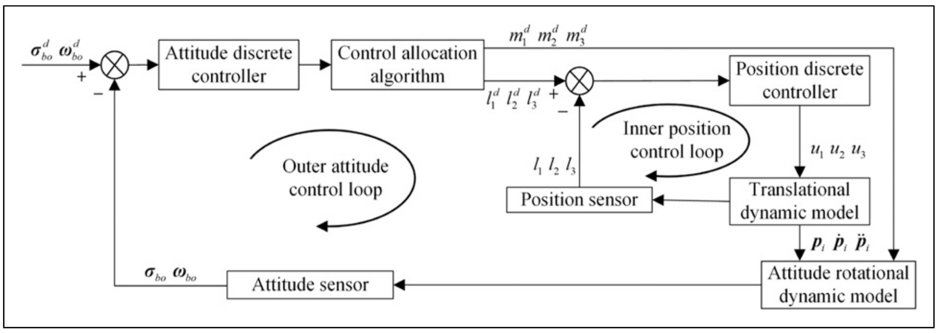

Figure 2. Flow diagram of the control system.

An auxiliary variable vector $\boldsymbol{z}$ is defined as[35]

$$\boldsymbol{z} = \widehat{\boldsymbol{d}} - K(\boldsymbol{J}_B + \boldsymbol{J}_M)\boldsymbol{\omega}_{bo} \tag{37}$$

Using the time derivative of equation (37) yields

$$\dot{\boldsymbol{z}} = \dot{\widehat{\boldsymbol{d}}} - K(\boldsymbol{J}_B + \boldsymbol{J}_M)\dot{\boldsymbol{\omega}}_{bo} \tag{38}$$

where

$$\begin{aligned}\dot{\widehat{\boldsymbol{d}}} = K\left(\boldsymbol{d} - \widehat{\boldsymbol{d}}\right) &= K[(\boldsymbol{I}_B + \boldsymbol{I}_M)\dot{\boldsymbol{\omega}}_{bo} + \boldsymbol{\omega}\times(\boldsymbol{I}_B + \boldsymbol{I}_M)\boldsymbol{\omega} \\ &-\boldsymbol{u}_t] - K(\boldsymbol{I}_B + \boldsymbol{I}_M)(\boldsymbol{\omega}_{bo}\times\boldsymbol{A}_{bo}\boldsymbol{\omega}_{oi}) - K\widehat{\boldsymbol{d}}\end{aligned} \tag{39}$$

Therefore, the nonlinear disturbance observer is given by

$$\begin{cases}\dot{\boldsymbol{z}} = K[(\boldsymbol{I}_B + \boldsymbol{I}_M)\dot{\boldsymbol{\omega}}_{bo} + \boldsymbol{\omega}\times(\boldsymbol{I}_B + \boldsymbol{I}_M)\boldsymbol{\omega}] \\ \quad - K[(\boldsymbol{I}_B + \boldsymbol{I}_M)(\boldsymbol{\omega}_{bo}\times\boldsymbol{A}_{bo}\boldsymbol{\omega}_{oi}) + \boldsymbol{u}_t] - K\widehat{\boldsymbol{d}} \\ \quad - K(\boldsymbol{I}_B + \boldsymbol{I}_M)\dot{\boldsymbol{\omega}}_{bo} = K[\boldsymbol{\omega}\times(\boldsymbol{I}_B + \boldsymbol{I}_M)\boldsymbol{\omega} \\ \quad - (\boldsymbol{I}_B + \boldsymbol{I}_M)(\boldsymbol{\omega}_{bo}\times\boldsymbol{A}_{bo}\boldsymbol{\omega}_{oi})] - K\boldsymbol{u}_t - K\widehat{\boldsymbol{d}} \\ \widehat{\boldsymbol{d}} = \boldsymbol{z} + K(\boldsymbol{I}_B + \boldsymbol{I}_M)\boldsymbol{\omega}_{bo}\end{cases} \tag{40}$$

Since the disturbance $\boldsymbol{d}$ varies slowly relative to the observer dynamics, it is reasonable to assume that $\dot{\boldsymbol{d}} = 0$; thus, this observer does not need prior information on the derivative of the disturbance.

The observer error is define as $\tilde{\boldsymbol{d}} = \boldsymbol{d} - \widehat{\boldsymbol{d}}$. By combining equation (36), the observer error equation is given by

$$\dot{\tilde{\boldsymbol{d}}} + K\tilde{\boldsymbol{d}} = 0 \tag{41}$$

The analytical solution of the observer error is

$$\tilde{\boldsymbol{d}}(t) = \tilde{\boldsymbol{d}}(t_0)e^{-Kt} \tag{42}$$

Thus, the observer is globally asymptotically stable and $\tilde{\boldsymbol{d}}$ converges to zero at an exponential rate. Because of the effective compensation, the outer controller provides an accurate response.

The attitude sampling sequence is defined as k_S, and the period of attitude discrete control is defined as T_S. The attitude error is defined as

$$\boldsymbol{e}(k_S) = \boldsymbol{\sigma}^d(k_S) - \boldsymbol{\sigma}(k_S) \tag{43}$$

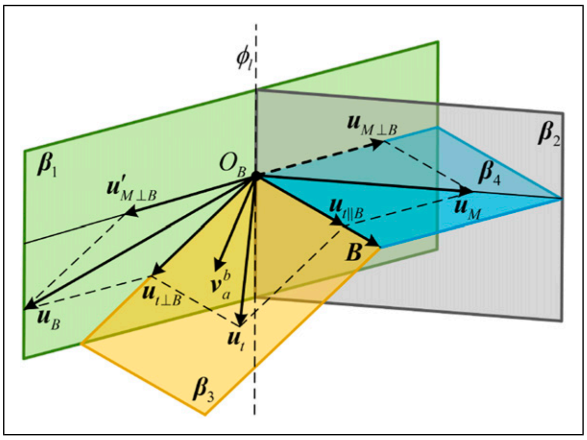

Figure 3. Allocation of the ideal control torque.

By combining the disturbance observer in equation (40), the Proportion Differential (PD) control law in the outer attitude control loop is given by

$$\boldsymbol{u}(k_S) = k_p^{\text{out}}\boldsymbol{e}(k_S) + k_d^{\text{out}}\frac{\boldsymbol{e}(k_S) - \boldsymbol{e}(k_S - 1)}{T_S} - \widehat{\boldsymbol{d}}(k_S) \tag{44}$$

where k_p^{out} and k_d^{out} are control parameters.

Control torque allocation algorithm

Since the control law is only designed for the ideal three-dimensional control torque, a control torque allocation algorithm is designed to obtain actual control inputs, which are the positions of moving masses and the magnetic moment of the magnetorquer.

The relative flow vector expressed in the $O_BX_BY_BZ_B$ system is defined as $\boldsymbol{v}_a^b$, and its unit vector is $\widehat{\boldsymbol{v}}_a^b$. As shown in Figure 3, the planes $\boldsymbol{\beta}_1$ and $\boldsymbol{\beta}_2$ are perpendicular to the geomagnetic field vector $\boldsymbol{B}$ and the relative flow vector $\widehat{\boldsymbol{v}}_a^b$, respectively. Line ϕ_l is the intersection of the planes $\boldsymbol{\beta}_1$ and $\boldsymbol{\beta}_2$. The control torque $\boldsymbol{u}_t$ on plane $\boldsymbol{\beta}_3$ can be decomposed as

$$\boldsymbol{u}_t = \boldsymbol{u}_{t\perp B} + \boldsymbol{u}_{t\|B} \tag{45}$$

where vector $\boldsymbol{u}_{t\|B}$ is parallel to vector $\boldsymbol{B}$, and vector $\boldsymbol{u}_{t\perp B}$ is on plane $\boldsymbol{B}$. According to the projection theorem, it yields

$$\boldsymbol{u}_{t\|B} = \widehat{\boldsymbol{B}}\left[\left(\widehat{\boldsymbol{B}}\right)^{\mathrm{T}}\boldsymbol{u}_t\right] \tag{46}$$

$$\boldsymbol{u}_{t\perp B} = \boldsymbol{u}_t - \boldsymbol{u}_{t\|B} \tag{47}$$

where $\widehat{\boldsymbol{B}}$ is the unit vector of $\boldsymbol{B}$.

Since the geomagnetic torque $\boldsymbol{u}_B$ is perpendicular to vector $\boldsymbol{B}$, vector $\boldsymbol{u}_{t\|B}$ is the projection of the aerodynamic torque vector $\boldsymbol{u}_M$ in the direction of vector $\widehat{\boldsymbol{B}}$. Vector $\boldsymbol{u}_{M\perp B}$ is the projection of vector $\boldsymbol{u}_M$ on plane $\boldsymbol{\beta}_1$. The sum of the vectors $\boldsymbol{u}_{t\perp B}$ and $\boldsymbol{u}'_{M\perp B}$, which is the opposite vector of $\boldsymbol{u}_{M\perp B}$, is the geomagnetic torque $\boldsymbol{u}_B$.

The plane perpendicular to plane $\boldsymbol{\beta}_2$ is defined as $\boldsymbol{\beta}_4$; thus, the aerodynamic torque $\boldsymbol{u}_M$ can be expressed as[17]

$$\boldsymbol{u}_M = \frac{\boldsymbol{u}_t^{\mathrm{T}}\widehat{\boldsymbol{B}}}{\left(\boldsymbol{P}\boldsymbol{u}_{t\|B}\right)^{\mathrm{T}}\widehat{\boldsymbol{B}}}\left(\boldsymbol{P}\boldsymbol{u}_{t\|B}\right), \quad \boldsymbol{P} = \boldsymbol{I}_{3\times 3} - \widehat{\boldsymbol{v}}_a^b\left(\widehat{\boldsymbol{v}}_a^b\right)^{\mathrm{T}} \tag{48}$$

Therefore, the position vector of the CoM of the system and the magnetic moment vector are given by

$$\boldsymbol{r}_s = -\frac{\boldsymbol{F}_{\text{aero}}\times\boldsymbol{u}_M}{\boldsymbol{F}_{\text{aero}}^2}, \quad \boldsymbol{m}_B = \frac{\boldsymbol{B}\times\boldsymbol{u}_B}{\boldsymbol{B}^2} \tag{49}$$

Simulation

A numerical simulation platform is developed in the Matlab/Simulink environment to verify the feasibility of using the moving mass actuator for attitude control and determine the effectiveness of the proposed double-loop discrete control law. A 2U CubeSat (110 mm × 110 mm ×

Table 1. Parameters of the CubeSat and controller.

Parameters	Value
Mass	$m_B = 1.55$ kg, $m_i = 0.15$ kg
Moment of inertia	$\boldsymbol{I}_B = \mathrm{diag}(0.003, 0.008, 0.008)$ $\mathrm{kg \cdot m^2}$
Limitation of magnetic moment	$\pm$ 0.05Am^2
Coefficient of aerodynamic force	$0.5\rho\Vert \boldsymbol{v}_a \Vert^2 C_D = 0.0018$
Orbit angular velocity	$\boldsymbol{\omega}_{oi} = [0, -0.0015, 0]^{\mathrm{T}}$ rad/s
Initial attitude	$[10, 30, -10]°$ $\boldsymbol{\omega}_{bo0} = [-0.005, 0.001, -0.006]^{\mathrm{T}}$ rad/s
Desired attitude	$[40, -10, 10]°$ $\boldsymbol{\omega}_{bod} = [0, 0, 0]^{\mathrm{T}}$ rad/s
Disturbances	$\triangle \boldsymbol{r}_s = [0.002, -0.001, 0.001]^{\mathrm{T}}$ m $\triangle \boldsymbol{F}_{aero} = \left[0.25\cos\left(\frac{\pi t}{2700}\right) + 0.05\right] \times \boldsymbol{F}_{aero}$, $\boldsymbol{m}_{rsd} = [0.005, 0.004, -0.003]^{\mathrm{T}}$ Am^2 $\boldsymbol{d}_s = [5, -5, -8]^{\mathrm{T}} \times 10^{-8}$ Nm
Orbital parameters	Orbit height: 350 km Orbit inclination: 96.68° Orbit period: 5492.1 s
Control parameters in inner loop	$k_p^{\mathrm{in}} = 0.05$, $k_i^{\mathrm{in}} = 0.025$, $k_d^{\mathrm{in}} = 0.018$ $\varepsilon = [0.001, 0.001, 0.001]^{\mathrm{T}}$, $T_p = 1$ s
Control parameters in outer loop	$k_p^{\mathrm{out}} = 2 \times 10^{-5}$, $k_d^{\mathrm{out}} = 4 \times 10^{-4}$ $K = 1$, $T_S = 10$ s

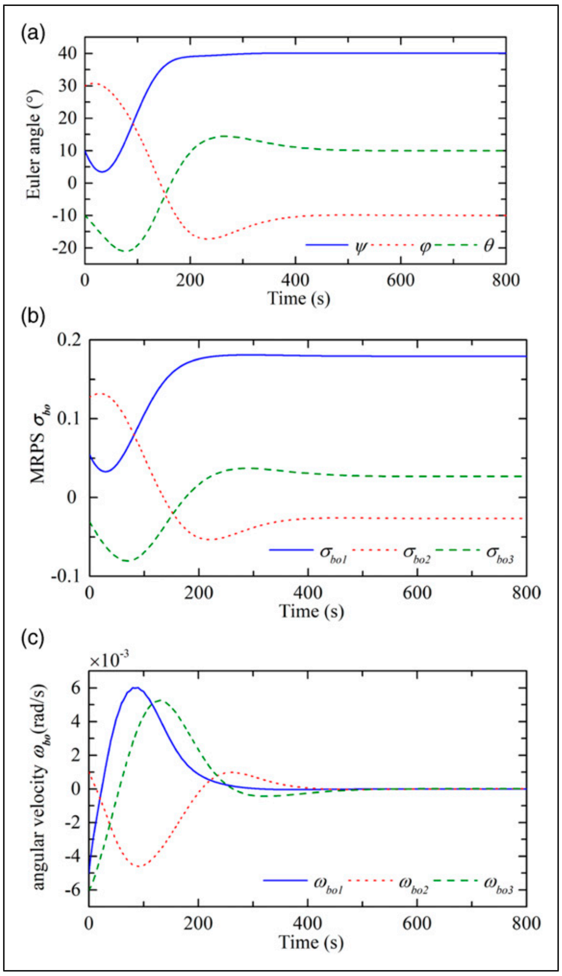

Figure 4. Curves of the attitude parameters. (a) Euler angle (ψ-yaw, θ-pitch, and φ-row); (b) MRPS; (c) angular velocity.

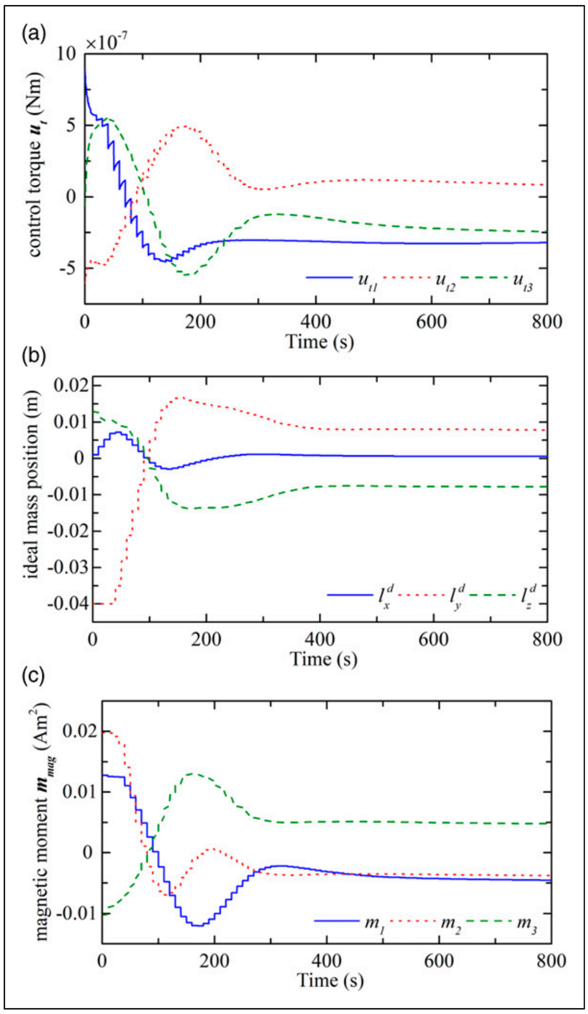

Figure 5. Curves of the control inputs. (a) Actual control torque; (b) ideal position of each mass; (c) magnetic moment.

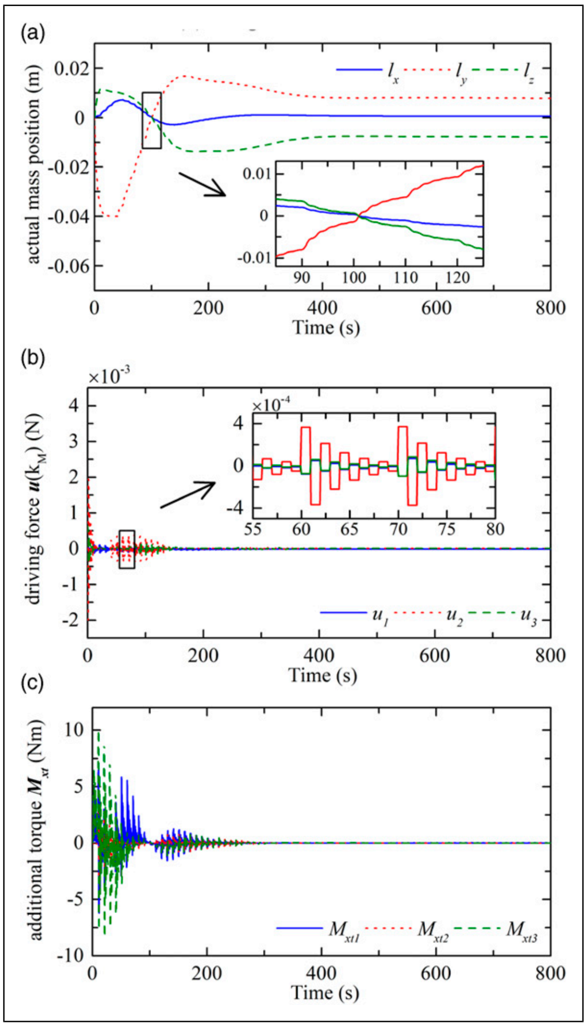

Figure 6. Curves of the actual movement of masses. (a) Actual position of each mass; (b) driving force of each linear motor; (c) additional torque caused by the moving masses.

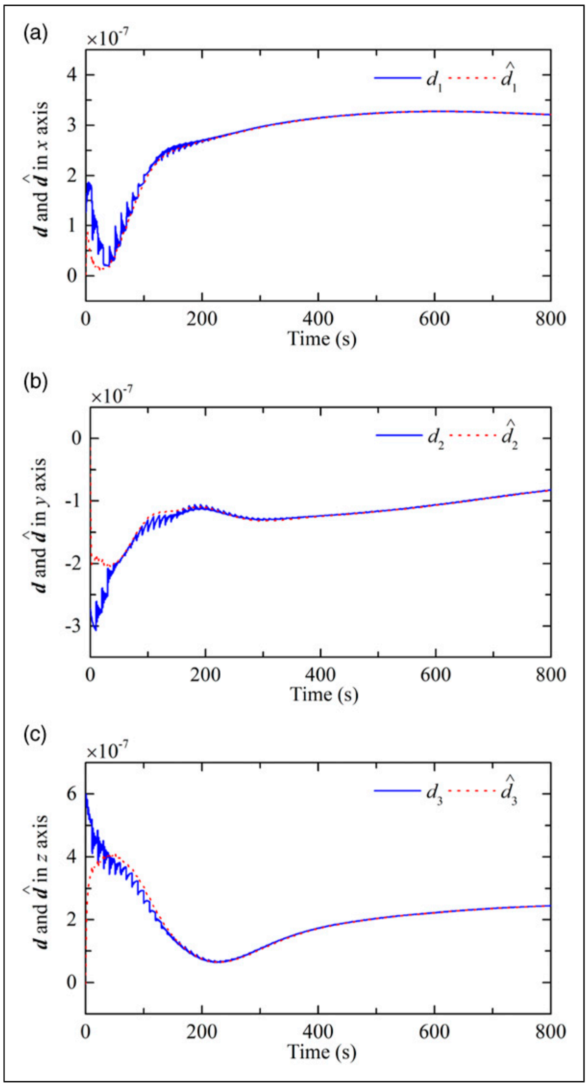

Figure 7. Tracking curves of the system disturbance. The units of the disturbance and its observed value are both Nm.

230 mm) was used as an example; the position vectors of three masses are $\boldsymbol{p}_1 = [l_1, 0.01, -0.01]^{\mathrm{T}}, \boldsymbol{p}_2 = [-0.01, l_2, 0.01]^{\mathrm{T}}$, and $\boldsymbol{p}_3 = [0.01, -0.01, l_3]^{\mathrm{T}}$. The given stroke limitation of each mass is ±40 mm; thus, the adjustable range of the CoM in three axes is ±3 mm. The parameters of the CubeSat and the proposed control scheme are listed in Table 1.

In the numerical simulation, the dynamic update period is 50 ms, and the total simulation time is 800 s. The disturbance observer is updated according to the measurement frequency, which is 2 Hz in this study. The ideal aerodynamic force is calculated by equation (26) according to the given aerodynamic parameters and the given surface characteristics. The simulation results are presented in Figures 4–7:

As shown in Figure 4, when the proposed double-loop controller is used, the CubeSat can complete the attitude maneuver in about 500 s, and the convergence accuracy of the Euler angle is up to ±0.1°. Thus, the proposed attitude control scheme is capable of controlling the attitude by using the aerodynamic torque and the magnetic torque. In addition, by selecting appropriate parameters of the PD controller in the outer attitude loop, the angle overshoot can be minimized, and the control effect can be optimized. However, there is a tradeoff between the overload of actuators and the attitude convergence speed.

As shown in Figure 5, the attitude control torque in the outer loop exhibits sudden changes due to the step change of the magnetic moment input. As shown in Figure 6(a) and (b), although the ideal positions of moving masses are step changing, the change in actual positions is smooth and gentle due to the discrete driving force calculated by the discrete PID controller in the inner loop. Thus, the additional disturbance of moving masses has been reduced to the order of 10^{-8} Nm, as shown in Figure 6(c); this disturbance is negligible compared to other disturbances and the control torque. However, since the actual control input of the motor is the driving force, there is a position deviation between the actual movement and the ideal position, which could result in a control torque error. An adjustment of the parameters of the PID controller in the inner loop can accelerate masses and reduce the control error; however, this would inevitably cause more serious problem of additional disturbances.

Since the positions of moving masses calculated by the control law has exceeded ±40 mm, as shown in Figure 6(a), the y-axis mass reaches its maximum, which also generates a control error. Thus, a large peak in the disturbance occurs before 50 s, as shown in Figure 7. Subsequently, as the control error decreases significantly, the change of the system disturbance tends to be slow time-varying. Ultimately, the control input stabilizes at about 350 s, but the control input fails to converge to 0 for compensating the system disturbance. In addition, due to the rapid changes in the positions of moving masses during the attitude maneuver, additional disturbances cause fluctuations in the disturbance and large errors of the observed value before 200 s. Therefore, the influence of additional disturbances is strong during attitude maneuvering.

Conclusions

In this study, an attitude control method of using the moving mass actuator was presented to solve the problem of strong aerodynamic disturbances in LEO. The dynamic effect was considered in the control system to further verify the feasibility of the proposed method. The rotational and translational equations derived for the CubeSat with a moving mass actuator indicated that the additional disturbance caused by the moving masses was a fast time-varying disturbance, which could be significantly reduced by slowing down the movement of moving masses. Thus, a discrete control algorithm was used to extend the control period. An integrated attitude control method using the moving mass system with a three-axis magnetorquer was used to prevent the underactuation of the system. A double-loop PID control scheme was designed to obtain the ideal three-dimensional control torque, which was then allocated to two actuators. The results of the numerical simulation revealed that the CubeSat could execute the attitude maneuvering despite the uncertain dynamics, unknown disturbances, and dynamic effects. Moreover, although the influence of additional disturbances was strong during attitude maneuvering, their effects were negligible compared with other disturbances and the control torque. Other unknown disturbances, which were slow time-varying, were precisely estimated by the disturbance observer. The results further verified the feasibility of using the moving mass actuator to control the attitude of the LEO CubeSat. However, this study only verified the feasibility of the integrated attitude control method using numerical simulation. In the future, more works will be done on the practical applications of the moving mass actuator.

Declaration of conflicting interests

The author(s) declared no potential conflicts of interest with respect to the research, authorship, and/or publication of this article.

Funding

The author(s) disclosed receipt of the following financial support for the research, authorship, and/or publication of this article: This work was supported in part by the National Natural Science Foundation of China under Grant 61803204, and in part by the Natural Science Foundation of Jiangsu Province under Grant BK20180465.

ORCID iDs

Zhengliang Lu, https://orcid.org/0000-0003-1856-5950
Yuandong Hu, https://orcid.org/0000-0002-1495-2876
Wenhe Liao, https://orcid.org/0000-0002-1710-4311

References

1. Lee ZT. *CubeSat constellation implementation and management using differential drag*. Master Dissertation. Boston: Massachusetts Institute of Technology, 2017.
2. Zhou W, Wang H, Ruan Z, et al. High accuracy attitude control system design for satellite with flexible appendages. *Math Probl Eng* 2014; 2014: 695758.
3. Miyata K, Kawashima R and Inamori T. Detailed analysis of aerodynamic effect on small satellites. *Trans Jpn Soc Aeronaut Space Sci* 2018; 16: 432–440.
4. Childs DW. A movable-mass attitude-stabilization system for artificial-g space stations. *J Spacecr Rockets* 1971; 8: 829–834.
5. Edwards TL and Kaplan MH. Automatic spacecraft detumbling by internal mass motion. *AIAA J* 1974; 12: 496–502.
6. Guo PF and Zhao LY. Modeling and attitude control of a spinning spacecraft with internal moving mass. *Adv Mat Res* 2013; 760-762: 1216–1220.
7. Kumar KD and Zou AM. Attitude control of miniature satellites using movable masses. In: SpaceOps 2010 Conference, Huntsville, AL, USA, 2010.
8. Atkins BM and Henderson TA. Under-actuated moving mass attitude control for a 3U Cubesat mission. In: 22nd Spaceflight Mechanics, Charleston, SC, USA, 2012, Vol. 143, 2083–2094.
9. Menon PK, Sweriduk GD, Ohlmeyer EJ, et al. Integrated guidance and control of moving-mass actuated kinetic warheads. *J Guid Control Dyn* 2004; 27: 118–126.
10. Zheng Q and Zhou Z. Stability of moving mass control spinning missiles with angular rate loops. *Math Probl Eng* 2019; 2019: 7832602.
11. Thomas S, Paluszek M, Wie B, et al. Design and simulation of sailcraft attitude control systems using the solar sail control toolbox. In: AIAA Guidance, Navigation, and Control Conference, Providence, RI, USA, 2004, 2004–4890.
12. Shahin F and Gong SP. Attitude control of a flexible solar sail in low Earth orbit. *J Guid Control Dyn* 2018; 41(8): 1715–1730.
13. Wie B. Solar sail attitude control and dynamics, part two. *J Guid Control Dyn* 2004; 27(4): 536–544.
14. Wie B and Murphy D. Solar-sail attitude control design for a flight validation mission. *J Spacecr Rockets* 2007; 44(4): 809–821.
15. Lu ZL. *Study on mass moment attitude control for fast orbit maneuver satellite*. PhD dissertation. Nanjing, China: Nanjing University of Science and Technology, 2017.
16. Chesi S. *Attitude control of nanosatellites using shifting masses*. Santa Cruz, China: University of California, 2015.
17. Chesi S, Gong Q and Romano M. Aerodynamic three-axis attitude stabilization of a spacecraft by center-of-mass shifting. *J Guid Control Dyn* 2017; 40(7): 1613–1626.

18. Virgili-liop J and Polat HC. Using shifting masses to reject aerodynamic perturbations and to maintain a stable attitude in very low earth orbit. In: 26th AAS/AIAA Space Flight Mechanics Meeting, Napa, CA, USA, 2016, 2129–2148.
19. Polat HC. *Prototype design and mission analysis for a small satellite exploiting environment disturbances for attitude stabilization*. PhD dissertation. Monterey, CA: Naval Postgraduate School, 2016.
20. Virgili-Liop J, Polat HC and Romano M. Attitude stabilization of spacecraft in very low earth orbit by center-of-mass shifting. *Front Robotics AI* 2019; 6: 7.
21. Robinett RD, Sturgis BR and Kerr SA. Moving mass trim control for aerospace vehicles. *J Guid Control Dyn* 1996; 19: 1064–1070.
22. Daniel HE. Dynamics and control of spinning spacecraft using translating masses with friction compensation. *J Spacecr Rockets* 2017; 54(6): 1376–1382.
23. Gutiérrez-Frias O, Martinez Garcia JC and Garrido R. PD control for vibration attenuation in a physical pendulum with moving mass. *Math Probl Eng* 2009; 2009: 179724.
24. El-Gohary AI and Tawfik TS. Optimal control of the rotational motion of a rigid body using moving masses. *Appl Math Comput* 2004; 153: 453–465.
25. Lu ZL and Zhang X. Mass moment attitude control system design for nano-satellite in orbital transition. *Acta Aeronautica Et Astrinautica Sinica* 2016; 38(6): 320778.
26. Ahn YT. *Attitude dynamics and control of a spacecraft using shifting mass distribution*. PhD dissertation. State College, PA, USA: The Pennsylvania State University, 2012.
27. Grubin C. Dynamics of a vehicle containing moving parts. *J Appl Mech* 1962; 29: 486–488.
28. Drob D, Emmert JT, Crowley G, et al. An empirical model of the Earth's horizontal wind fields: HWM07. *J Geophys Res Space Phys* 2008; 113: 13029.
29. Psiaki ML. Nanosatellite attitude stabilization using passive aerodynamics and active magnetic torquing. *J Guid Control Dyn* 2004; 27(3): 347–355.
30. Lovera M, De Marchi E and Bittanti S. Periodic attitude control techniques for small satellites with magnetic actuators. *IEEE Trans Contr Syst Technol* 2002; 10(1): 90–95.
31. Chesi S, Gong Q, Pellegrini V, et al. Automatic mass balancing of a spacecraft three-axis simulator: analysis and experimentation. *J Guid Control Dyn* 2014; 37(1): 197–206.
32. Khan HS and Kadri MB. Attitude and altitude control of quadrotor by discrete PID control and non-linear model predictive control. In: 2015 International Conference on Information and Communication Technologies (ICICT), Karachi, Pakistan, 12–13 December 2015, 1–11.
33. Hodel AS and Hall CE. Variable-structure PID control to prevent integrator windup. *IEEE Trans Ind Electron* 2001; 48: 442–451.
34. Hu Q, Li B and Qi J. Disturbance observer based finite-time attitude control for rigid spacecraft under input saturation. *Aerosp Sci Technol* 2014; 39: 13–21.
35. Wen-Hua Chen WH, Ballance DJ, Gawthrop PJ, et al. A nonlinear disturbance observer for robotic manipulators. *IEEE Trans Ind Electron* 2000; 47(4): 932–938.

Appendix

By combining equation (17) and the definitions $\boldsymbol{p}_1 = [l_1, \delta_{12}, \delta_{13}]^{\mathrm{T}}$, $\boldsymbol{p}_2 = [\delta_{21}, l_2, \delta_{23}]^{\mathrm{T}}$, $\boldsymbol{p}_3 = [\delta_{31}, \delta_{31}, l_3]^{\mathrm{T}}$, and $\boldsymbol{\omega}_B = [\omega_1, \omega_2, \omega_3]^{\mathrm{T}}$, the scalar expansion form of the translational dynamic equation of each mass can be stated as

$$\begin{aligned}
\ddot{l}_1 = \frac{1}{M+m_2+m_3}\Big[&(M+m_1+m_2+m_3)u_1/m_1 - F_{e1} \\
&-(M+m_1+m_2+m_3)(-\dot{\omega}_3\delta_{12} + \dot{\omega}_2(-\dot{\omega}_2 l_1 \\
&+\dot{\omega}_1\delta_{12}) + \dot{\omega}_2\delta_{13} - \dot{\omega}_3(\dot{\omega}_3 l_1 - \dot{\omega}_1\delta_{13})) \\
&+m_1(-\dot{\omega}_3\delta_{12} + \dot{\omega}_2(-\dot{\omega}_2 l_1 + \dot{\omega}_1\delta_{12}) \\
&+\dot{\omega}_2\delta_{13} - \dot{\omega}_3(\dot{\omega}_3 l_1 - \dot{\omega}_1\delta_{13})) \\
&+m_3\big(\dot{\omega}_2 l_3 - \dot{\omega}_3(-\dot{\omega}_1 l_3 + \dot{\omega}_3\delta_{31}) - \dot{\omega}_3\delta_{32} \\
&+\dot{\omega}_2(-\dot{\omega}_2\delta_{31} + \dot{\omega}_1\delta_{32}) + 2\dot{l}_3\omega_2\big) \\
&+m_2\big(-\dot{\omega}_3 l_2 + \dot{\omega}_2(\dot{\omega}_1 l_2 - \dot{\omega}_2\delta_{21}) \\
&+\dot{\omega}_2\delta_{23} - \dot{\omega}_3(\dot{\omega}_3\delta_{21} - \dot{\omega}_1\delta_{23}) - 2\dot{l}_2\omega_3\big)\Big]
\end{aligned} \tag{50}$$

$$\begin{aligned}
\ddot{l}_2 = \frac{1}{M+m_1+m_3}\Big[&(M+m_1+m_2+m_3)u_2/m_2 - F_{e2} \\
&-(M+m_1+m_2+m_3)(\dot{\omega}_3\delta_{21} - \dot{\omega}_1(\dot{\omega}_1 l_2 \\
&-\dot{\omega}_2\delta_{21}) - \dot{\omega}_1\delta_{23} + \dot{\omega}_3(-\dot{\omega}_3 l_2 + \dot{\omega}_2\delta_{23})) \\
&+m_2(\dot{\omega}_3\delta_{21} - \dot{\omega}_1(\dot{\omega}_1 l_2 - \dot{\omega}_2\delta_{21}) - \dot{\omega}_1\delta_{23} \\
&+\dot{\omega}_3(-\dot{\omega}_3 l_2 + \dot{\omega}_2\delta_{23})) + m_3\big(-\dot{\omega}_1 l_3 \\
&+\dot{\omega}_3\delta_{31} - \dot{\omega}_1(-\dot{\omega}_2\delta_{31} + \dot{\omega}_1\delta_{32}) \\
&+\dot{\omega}_3(\dot{\omega}_2 l_3 - \dot{\omega}_3\delta_{32}) - 2\dot{l}_3\omega_1\big) \\
&+m_1\big(\dot{\omega}_3 l_1 - \dot{\omega}_1(-\dot{\omega}_2 l_1 + \dot{\omega}_1\delta_{12}) - \dot{\omega}_1\delta_{13} \\
&+\dot{\omega}_3(-\dot{\omega}_3\delta_{12} + \dot{\omega}_2\delta_{13}) + 2\dot{l}_1\omega_3\big)\Big]
\end{aligned} \tag{51}$$

$$\begin{aligned}
\ddot{l}_3 = \frac{1}{M+m_1+m_2}\Big[&(M+m_1+m_2+m_3)u_3/m_3 - F_{e3} \\
&-(M+m_1+m_2+m_3)(-\dot{\omega}_2\delta_{31} + \dot{\omega}_1(-\dot{\omega}_1 l_3 \\
&+\dot{\omega}_3\delta_{31}) + \dot{\omega}_1\delta_{32} - \dot{\omega}_2(\dot{\omega}_2 l_3 - \dot{\omega}_3\delta_{32})) \\
&+m_3(-\dot{\omega}_2\delta_{31} + \dot{\omega}_1(-\dot{\omega}_1 l_3 + \dot{\omega}_3\delta_{31}) \\
&+\dot{\omega}_1\delta_{32} - \dot{\omega}_2(\dot{\omega}_2 l_3 - \dot{\omega}_3\delta_{32})) \\
&+m_2\big(\dot{\omega}_1 l_2 - \dot{\omega}_2\delta_{21} + \dot{\omega}_1(\dot{\omega}_3\delta_{21} - \dot{\omega}_1\delta_{23}) \\
&-\dot{\omega}_2(-\dot{\omega}_3 l_2 + \dot{\omega}_2\delta_{23}) + 2\dot{l}_2\omega_1\big) \\
&+m_1\big(-\dot{\omega}_2 l_1 + \dot{\omega}_1\delta_{12} + \dot{\omega}_1(\dot{\omega}_3 l_1 - \dot{\omega}_1\delta_{13}) \\
&-\dot{\omega}_2(-\dot{\omega}_3\delta_{12} + \dot{\omega}_2\delta_{13}) - 2\dot{l}_1\omega_2\big)\Big]
\end{aligned} \tag{52}$$